



Ag₂C₂O₄ and Ag₂C₂O₄/TiO₂ nanocomposites as highly efficient and stable photocatalyst under visible light: Preparation, characterization and photocatalytic mechanism



Caixia Feng^a, Mingming Sun^a, Yan Wang^{a,c,*}, Xianshun Huang^a, Anchao Zhang^{b,**}, Yuhua Pang^a, Yanmei Zhou^a, Linshan Peng^a, Yanting Ding^a, Ling Zhang^a, Deliang Li^a

^a Institute of Environmental and Analytical Sciences, College of Chemistry and Chemical Engineering, Henan University, Kaifeng 475004, China

^b School of Mechanical and Power Engineering, Henan Polytechnic University, Jiaozuo 454000, China

^c Department of Scientific Research, Henan University, Kaifeng 475004, China

ARTICLE INFO

Article history:

Received 31 May 2017

Received in revised form 23 June 2017

Accepted 26 July 2017

Available online 4 August 2017

Keywords:

Ag₂C₂O₄/TiO₂

Photo-corrosion

Visible light

Plasma resonance

Photocatalytic activity

ABSTRACT

Ag₂C₂O₄ and Ag₂C₂O₄/TiO₂ (Commercial P25-TiO₂) nanocomposites with different weight ratios of Ag₂C₂O₄ to P25-TiO₂ (denoted as Ag₂C₂O₄/TiO₂-0.02, Ag₂C₂O₄/TiO₂-0.08, Ag₂C₂O₄/TiO₂-0.15, Ag₂C₂O₄/TiO₂-0.25, Ag₂C₂O₄/TiO₂-0.3) were synthesized by a facile liquid precipitation method. The photocatalytic activity of samples was evaluated by the degradation of propylene and acetaldehyde gas under visible light irradiation. All the samples displayed a highly efficient and stable photocatalytic activity. Furthermore, compared to pure Ag₂C₂O₄ and P25-TiO₂ (used as reference), Ag₂C₂O₄/TiO₂ nanocomposites showed much higher photocatalytic activity and Ag₂C₂O₄/TiO₂-0.25 possessed the highest photocatalytic activity. The kinetic behavior of Ag₂C₂O₄/TiO₂-0.25 was well accordant with a pseudo-first-order reaction and the reaction rate constants were calculated to be 11.13 h⁻¹ and 0.5376 h⁻¹ for the degradation of propylene and acetaldehyde, respectively. The mechanism of highly efficient and stable photocatalytic activity was discussed. On the one hand, Ag₂C₂O₄ undergoes firstly photo-corrosion during the initial photocatalytic process generating nascent metallic Ag on the surface of Ag₂C₂O₄, which subsequently endowing the Ag@Ag₂C₂O₄ with visible light photocatalytic activity due to the plasma resonance of Ag. On the other hand, Ag₂C₂O₄/TiO₂ nanocomposites also experience the same journey resulting in the formation of Ag@Ag₂C₂O₄/TiO₂. Differently from Ag@Ag₂C₂O₄, two paths are involved to separate the electron and hole excited by the photon of nascent metallic Ag so as to acquire much higher photocatalytic activity for Ag@Ag₂C₂O₄/TiO₂.

© 2017 Elsevier B.V. All rights reserved.

1. Introduction

In recent years, many silver-containing photocatalytic materials have received great attention due to their proper band gap and relatively good performance in degradation of pollutants [1–7]. In 2008, Huang et al. synthesized Ag@AgCl as highly efficient and stable photocatalyst capable of photooxidation of methylic orange under visible light. They attributed the photocatalytic activity to the plasmon resonance of silver deposited on AgCl particles [1]. Ye

et al. reported the use of Ag₃PO₄ as an active visible-light-driven photocatalyst for the oxidation of water and photodecomposition of organic compounds. It was proposed that the p-block elements are actually important ingredients for high photocatalytic activity [4]. Adhering to this idea, Huang et al. prepared silver carbonate (Ag₂CO₃) short rods using a precipitation method. The prepared Ag₂CO₃ displayed a high activity towards degradation of phenol and methylene blue under visible light [5]. Dong et al. also reported the high-efficiency visible-light sensitive Ag₂CO₃ photocatalyst prepared by a simple ion-exchange method based on a strategy incorporating of p-block C element into a narrow bandgap Ag₂O. The theory calculation based on the plane-wave-based DFT indicates the incorporation of p-block C element into narrow bandgap Ag₂O broadens the bandgap width and enhances photodegradation ability [6].

* Corresponding author at: Institute of Environmental and Analytical Sciences, College of Chemistry and Chemical Engineering, Henan University, Kaifeng 475004, China.

** Corresponding author.

E-mail addresses: wangyan8079@vip.henu.edu.cn (Y. Wang), anchaozhang@126.com (A. Zhang).

However, these Ag-based photocatalysts usually experience photo-corrosion under visible light irradiation, which causes damage to their photocatalytic activity and thus, their practical applications are limited. To improve the photocatalytic activity and stability of silver-containing catalysts, many attempts have been performed to prevent the photo-corrosion and enhance the photocatalytic activity. One way is to add sacrificial agent as an electron acceptor in the reaction system [4,5,8]. Dai et al. investigated the photo-corrosion mechanism of Ag_2CO_3 in aqueous solution and proposed that the photocorrosion of Ag_2CO_3 can be efficiently inhibited by adding AgNO_3 in the photocatalytic reaction system owing to the lower electrode potential of Ag/AgNO_3 than that of $\text{Ag}/\text{Ag}_2\text{CO}_3$ [8]. Another widely used way is coupling the Ag-based photocatalysts with each other or other semiconductor materials to fabricate heterostructured photocatalysts [9–24]. On the one hand, Yu et al. coupled AgI into Ag_2CO_3 , generating novel $\text{AgI}/\text{Ag}_2\text{CO}_3$ composite photocatalyst. The formation of $\text{AgI}/\text{Ag}_2\text{CO}_3$ heterojunction with intimate interface could effectively increase the separation efficiency of the e^-/h^+ pairs and promote the production of $\cdot\text{OH}$ and $\text{O}_2^\bullet-$ radicals, which is beneficial to the photocatalytic degradation of MO [19]. Graphene interfaced with Ag_3PO_4 , Ag_3VO_4 , or Ag_2CO_3 were systematically studied and graphene was proposed as an excellent electron acceptor and transporter, which markedly promoted the separation of photoexcited electron–hole pairs [15,17,18]. On the other hand, TiO_2 sensitized by Ag-containing photocatalysts were achieved to enhance the stability and photocatalytic efficiency. Rawal et al. synthesized $\text{Ag}_3\text{PO}_4/\text{TiO}_2$ by covering the surface of Ag_3PO_4 with polycrystalline TiO_2 via sol-gel method. The remarkable photocatalytic activity of $\text{Ag}_3\text{PO}_4/\text{TiO}_2$ was attributed to the inter-semiconductor hole-transfer between the valence band of Ag_3PO_4 and TiO_2 [12]. Yu et al. found that coupling of trace Ag_2CO_3 with TiO_2 could enrich the surface OH groups of the sample and suppress the recombination rate of photogenerated electrons (e^-) and holes (h^+) pairs [13]. Mohaghegh et al. reported that Ag_2CO_3 sensitized TiO_2 prepared in ionic liquid medium formed the $\text{Ag}_2\text{CO}_3/\text{TiO}_2/\text{RTIL}$ (2-hydroxyethylammonium formate) heterostructure affording to the promoted absorption of light and more efficient suppression of charge carrier recombination [14]. In our previous work, anatase TiO_2 containing a large amount of single-electron-trapped oxygen vacancy (denoted as $\text{TiO}_2(\text{V}_0^\bullet)$; V_0^\bullet refers to single-electron-trapped oxygen vacancies which are abridged as SETOVs) or P25- TiO_2 was combined with Ag_2CO_3 to prepare $\text{Ag}_2\text{CO}_3/\text{TiO}_2(\text{V}_0^\bullet)$ or $\text{Ag}_2\text{CO}_3/\text{P}25$ by the precipitation method [25–27]. The synergistic effect between the oxygen vacancies and nascent metallic Ag accounts for the high and stable photocatalytic activity of $\text{Ag}_2\text{CO}_3/\text{TiO}_2(\text{V}_0^\bullet)$ [25], while the synergistic effect between surface plasma resonance of silver and interfacial electron transfer is in favor of the enhanced photocatalytic performance of $\text{Ag}_2\text{CO}_3/\text{P}25$ [27]. In Ref. [26], we accidentally found that wide band gap semiconductor $\text{Ag}_2\text{C}_2\text{O}_4$ also showed highly efficient and stable visible light photocatalytic activity. As far as we know, no one has been reported that $\text{Ag}_2\text{C}_2\text{O}_4$ could be used as visible-light-active photocatalyst and its physicochemical properties, photo-corrosion, visible light photocatalytic behavior as well as photocatalytic mechanism should be further systematically studied.

In the present work, pure $\text{Ag}_2\text{C}_2\text{O}_4$ and a series of $\text{Ag}_2\text{C}_2\text{O}_4/\text{TiO}_2$ heterostructures with different weight ratios of $\text{Ag}_2\text{C}_2\text{O}_4$ to P25- TiO_2 were prepared by a facial precipitation method. The resulting $\text{Ag}_2\text{C}_2\text{O}_4$ and $\text{Ag}_2\text{C}_2\text{O}_4/\text{TiO}_2$ nanocomposite was characterized by means of scanning electron microscope (SEM), transmission electron microscope (TEM), X-ray diffraction (XRD), X-ray photoelectron spectroscopy (XPS). The comparison of XPS and XRD results of $\text{Ag}_2\text{C}_2\text{O}_4$ and $\text{Ag}_2\text{C}_2\text{O}_4/\text{TiO}_2$ between before and after irradiation suggested that both pure $\text{Ag}_2\text{C}_2\text{O}_4$ and ingredient $\text{Ag}_2\text{C}_2\text{O}_4$

of $\text{Ag}_2\text{C}_2\text{O}_4/\text{TiO}_2$ endured photo-corrosion to some extents generating nascent metallic Ag. As well known, such a photo-corrosion is originally non-conducive to the photocatalysts. However, both $\text{Ag}_2\text{C}_2\text{O}_4$ and $\text{Ag}_2\text{C}_2\text{O}_4/\text{TiO}_2$ nanocomposite showed highly efficient and stable photocatalytic activity toward the degradation of propylene and acetaldehyde gas under visible light. Compared to pure $\text{Ag}_2\text{C}_2\text{O}_4$ and P25- TiO_2 , $\text{Ag}_2\text{C}_2\text{O}_4/\text{TiO}_2$ heterostructures noticeably exhibited an improvement in both light absorption and photoactivity. The photocatalytic mechanisms of $\text{Ag}_2\text{C}_2\text{O}_4$ and $\text{Ag}_2\text{C}_2\text{O}_4/\text{TiO}_2$ were discussed in detail and proposed in this paper.

2. Experimental

All chemicals are of analytical grade purity and were used without further purification.

2.1. Catalysts preparation

$\text{Ag}_2\text{C}_2\text{O}_4$ was chemically synthesized by direct reaction in the aqueous solutions between AgNO_3 and $\text{Na}_2\text{C}_2\text{O}_4$ as the starting materials. Briefly, 5 mL of $\text{Na}_2\text{C}_2\text{O}_4$ (0.1 M) was added into a 50-mL beaker. Into $\text{Na}_2\text{C}_2\text{O}_4$ solution was then slowly added 15 mL of AgNO_3 (0.1 M) under 20 min of magnetic stirring to afford white precipitate $\text{Ag}_2\text{C}_2\text{O}_4$. As-obtained $\text{Ag}_2\text{C}_2\text{O}_4$ was filtered, washed with distilled water, and dried at 60 °C in dark.

$\text{Ag}_2\text{C}_2\text{O}_4/\text{TiO}_2$ nanocomposite photocatalysts were synthesized by an in-situ deposition of $\text{Ag}_2\text{C}_2\text{O}_4$ onto the surface of P25- TiO_2 . Briefly, 0.5 g of P25- TiO_2 powder was dispersed in distilled water and mixed with a quantity of $\text{Na}_2\text{C}_2\text{O}_4$ solution (0.05 M) under 10 min of magnetic stirring to afford a uniform suspension. Into the above mixed suspension was dripped an equal volume of AgNO_3 (0.1 M) solution under 20 min of magnetic stirring to yield the precipitate. The resultant precipitate was filtered, washed with distilled water, and dried at 60 °C in dark in an oven to provide disired $\text{Ag}_2\text{C}_2\text{O}_4/\text{TiO}_2$ nanocomposite. The produced $\text{Ag}_2\text{C}_2\text{O}_4/\text{TiO}_2$ nanocomposites with different theoretical weight ratios ($\text{Ag}_2\text{C}_2\text{O}_4:\text{P}25$) of 0.02:1, 0.08:1, 0.15:1, 0.25:1, 0.3:1 were named as $\text{Ag}_2\text{C}_2\text{O}_4/\text{TiO}_2-0.02$, $\text{Ag}_2\text{C}_2\text{O}_4/\text{TiO}_2-0.08$, $\text{Ag}_2\text{C}_2\text{O}_4/\text{TiO}_2-0.15$, $\text{Ag}_2\text{C}_2\text{O}_4/\text{TiO}_2-0.25$, $\text{Ag}_2\text{C}_2\text{O}_4/\text{TiO}_2-0.3$, respectively.

2.2. Characterization

The morphology of as-prepared photocatalysts was examined using field emission scanning electron microscopy (SEM, JEOL JSM-7610F) and transmission electron microscopy (TEM, JEM-2010). The crystal phase compositions of samples were measured with a Bruker D8 X-ray diffractometer (XRD) with $\text{Cu K}\alpha$ radiation at an accelerating voltage of 40 kV. The ultraviolet-visible light diffusion reflectance spectra (DRS) of the photocatalysts were recorded with a PE Lambda 950 spectrometer equipped with an integrating sphere attachment (BaSO_4 was used as a reference). X-ray photoelectron spectroscopy (XPS) measurements were performed on a Kratos AXIS system with a monochromatic $\text{Al-K}\alpha$ source ($h\nu = 1486.6 \text{ eV}$). The binding energies were calibrated with reference to adventitious C 1s line at 284.8 eV.

The photocurrent was carried out by electrochemical station (CHI 650E Chenhua Instrument Company) in a three-electrode quartz cell with 0.1 mol L^{-1} Na_2SO_4 electrolyte solution. A xenon lamp equipped with an ultraviolet cutoff filter was served as the visible light source ($>420 \text{ nm}$; light intensity: 1 mW cm^{-2}). A platinum wire and Ag/AgCl were used as counter electrode and reference electrode, respectively. The working electrode was prepared as follows: 2 mg of sample, 30 μL of water and 5 μL of Nafion were mixed to form homogeneous slurry. The resultant slurry was dropped onto the precleaned ITO glass and dried at room temperature for 12 h.

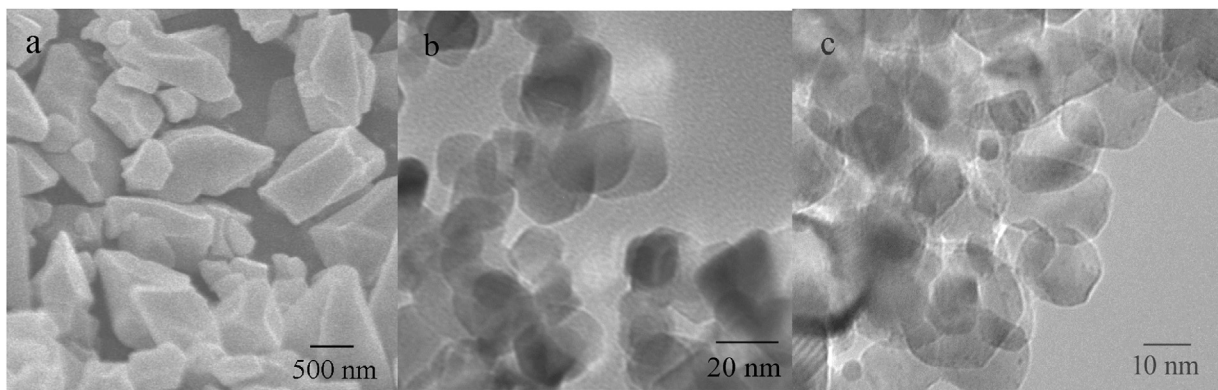


Fig. 1. SEM image (a) of $\text{Ag}_2\text{C}_2\text{O}_4$ and representative TEM images of P25-TiO₂ (b) and $\text{Ag}_2\text{C}_2\text{O}_4/\text{TiO}_2$ -0.25 (c) before irradiation.

2.3. Evaluation of visible light photocatalytic activity

The experiment of photo-degradation of propylene was performed in an on-line analysis system (denoted as system I) equipped with a gas chromatograph (GC7900) to monitor the concentration change of C_3H_6 (C), which has been reported elsewhere in our previous work [28]. In system I, 25 mg aliquot of each sample was spread on one side of a roughened glass plate (ca. 10 cm²) located in a quartz tube reactor equipped with a 300 W xenon lamp as the visible light source. Between the xenon lamp and reactor was inserted an ultraviolet (UV) cut 420 filter to eliminate UV light. The reactor was surrounded by a water channel so as to eliminate infrared light and keep a constant reaction temperature at room temperature. The feed gas was mixed of propylene and dry air, and was allowed to flow through the reactor at a flow rate of 200 mL h⁻¹. Prior to irradiation, the feed gas was allowed to flow through the reactor continuously until the adsorption/desorption equilibrium was established. The concentrations of C_3H_6 and CO_2 production were measured by GC equipped with a flame ionization detector (FID), a GDX-502 column, and a reactor loaded with Ni catalyst for methanization of CO_2 . The removal rate of C_3H_6 is calculated as $(C_0 - C)/C_0 \times 100\%$, where C_0 refers to the initial C_3H_6 concentration with a value of 500 ppmV.

The experiment of photo-degradation of acetaldehyde gas was performed in a steady state photocatalytic system (denoted as system II). In system II, as-evaluated catalysts was uniformly spread on the bottom of a quartz cylindrical reactor with a build-in port for collecting the inside feed gas. The feed gas is made up of acetaldehyde gas and dry air with a theoretically-calculated acetaldehyde gas concentration of 800 ppmV. The same optical source kept with a 25 cm distance above to the as-evaluated catalysts was used as the visible light source. At given intervals of irradiation, 1 mL of the feed gas was drawn off from the build-in port and immediately injected into the gas chromatograph to measure the concentration of acetaldehyde gas.

3. Results and discussion

3.1. Morphology and structure

The SEM and TEM images of $\text{Ag}_2\text{C}_2\text{O}_4$, P25-TiO₂ and $\text{Ag}_2\text{C}_2\text{O}_4/\text{TiO}_2$ nanocomposites are shown in Fig. 1. It can be seen from Fig. 1a that the size of $\text{Ag}_2\text{C}_2\text{O}_4$ is unsurprisingly located in micron scale fluctuating from 0.5 to 3 μm due to the simple precipitation method and the surface is relatively smooth. It is well known that P25-TiO₂ samples are consist of nanoparticles with a diameter of 20–30 nm, which is well in accordance with the results shown in Fig. 1b. As for $\text{Ag}_2\text{C}_2\text{O}_4/\text{TiO}_2$ nanocomposites, the morphology of P25-TiO₂ shown in Fig. 1c is almost unchanged. Surprisingly,

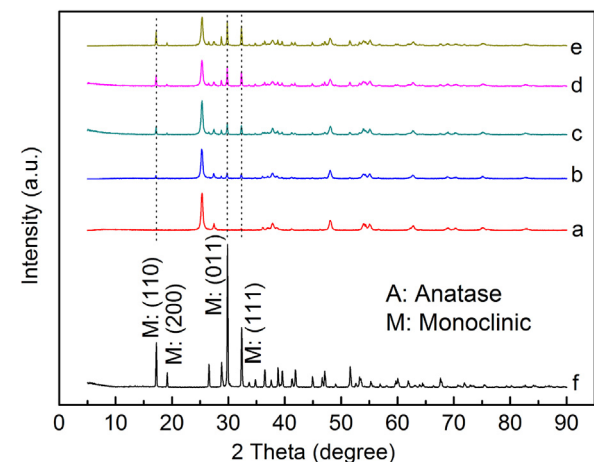
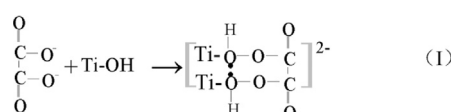


Fig. 2. XRD patterns of different photocatalysts: (a) $\text{Ag}_2\text{C}_2\text{O}_4/\text{TiO}_2$ -0.02, (b) $\text{Ag}_2\text{C}_2\text{O}_4/\text{TiO}_2$ -0.08, (c) $\text{Ag}_2\text{C}_2\text{O}_4/\text{TiO}_2$ -0.15, (d) $\text{Ag}_2\text{C}_2\text{O}_4/\text{TiO}_2$ -0.25, (e) $\text{Ag}_2\text{C}_2\text{O}_4/\text{TiO}_2$ -0.3, (f) $\text{Ag}_2\text{C}_2\text{O}_4$.

one could see that superfine $\text{Ag}_2\text{C}_2\text{O}_4$ with the size of 1–2 nm was well formed and dispersed on the surface of P25-TiO₂. Compared with the synthetic process of pure $\text{Ag}_2\text{C}_2\text{O}_4$, some chemical interaction must have been occurred between P25-TiO₂ with $\text{Na}_2\text{C}_2\text{O}_4$ before dripping into AgNO_3 solution. It is well known that there are valance-unfilled Ti(IV) ion centers and O(II) centers which form basic $\equiv\text{TiOH}$ and acidic $\equiv\text{OH}$ on the P25-TiO₂ particle surface in aqueous solution, respectively [29]. Therefore, it could be referred that oxalate ion may interact with basic $\equiv\text{TiOH}$ as follows:



When AgNO_3 solution was dripped into above mixture, oxalate ion would be robbed by Ag^+ and gradually released to generate superfine $\text{Ag}_2\text{C}_2\text{O}_4$ due to the slow-release effect. Taking into the value of solubility product constant ($K_{\text{sp}}(\text{Ag}_2\text{C}_2\text{O}_4) = 3.5 \times 10^{-11} \ll K_{\text{sp}}(\text{AgOH}) = 2.0 \times 10^{-8}$), it can be confirmed that the product was $\text{Ag}_2\text{C}_2\text{O}_4$ rather than AgOH or Ag_2O (transformed from AgOH).

Fig. 2 shows the XRD patterns of pure $\text{Ag}_2\text{C}_2\text{O}_4$ and $\text{Ag}_2\text{C}_2\text{O}_4/\text{TiO}_2$ nanocomposites with different weight ratios of TiO_2 to $\text{Ag}_2\text{C}_2\text{O}_4$. On the one hand, it can be seen from Fig. 2 (curve f) that the pure $\text{Ag}_2\text{C}_2\text{O}_4$ displayed obvious diffraction peaks at $2\theta = 17.15^\circ$, 19.21° , 29.94° and 32.38° , which can be indexed to the crystallite planes of (110), (200), (011) and (111) in monoclinic phase of $\text{Ag}_2\text{C}_2\text{O}_4$ (JCPDS No: 22-1335). On the other hand,

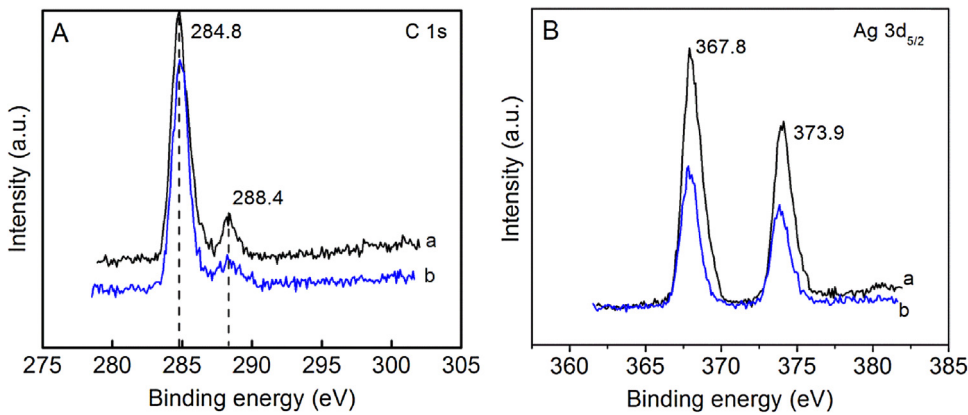


Fig. 3. High-resolution XPS spectra of C 1s (A) and Ag 3d (B) for $\text{Ag}_2\text{C}_2\text{O}_4$ (a) and $\text{Ag}_2\text{C}_2\text{O}_4/\text{TiO}_2$ -0.25 (b).

P25-TiO₂ is well known composed of anatase TiO₂ as the major phase and rutile TiO₂ as the minor phase (not given here) [30]. After Ag₂C₂O₄ was incorporated into P25-TiO₂, the Ag₂C₂O₄/TiO₂ nanocomposites displayed a miscible structure covering monoclinic phase Ag₂C₂O₄ mixed with anatase phase as well as rutile phase of P25-TiO₂, indicating that Ag₂C₂O₄ have been deposited on the surface of P25-TiO₂ (see curves b–e). Furthermore, with the increase of the ratio of Ag₂C₂O₄ to TiO₂ from 0.02:1 to 0.3:1, the intensity of monoclinic diffraction peaks of (110), (200), (011) and (111) improved remarkably and the others diffraction peaks gradually appeared.

3.2. XPS analysis

The X-ray photoelectron spectroscopy (XPS) was carried out to further investigate the composition and the chemical status of samples. Fig. 3A and B demonstrates the C 1s and Ag 3d XPS spectra of both Ag₂C₂O₄ and Ag₂C₂O₄/TiO₂-0.25 nanocomposite (possess the best photocatalytic performance), respectively. For both samples, the high resolution C 1s spectra display two peaks locating at 284.8 and 288.4 eV (see Fig. 3A), respectively. The former main peak can be assigned to carbon contamination from XPS instrument, while the latter peak is derived from the carbon element in Ag₂C₂O₄ [27]. Fig. 3B exhibits the narrow scan spectrum of Ag 3d at the binding energy of 367.8 eV (Ag 3d_{5/2}) and 373.9 eV (Ag 3d_{3/2}) with an energy splitting of ca. 6.1 eV, which are well consistent with the values reported for Ag⁺ ions [13,19,31], excluding the presence of any Ag⁰ species in both fresh samples.

3.3. Optical property analysis

The UV-vis absorption spectra of Ag₂C₂O₄, P25-TiO₂, and Ag₂C₂O₄/TiO₂ nanocomposites are given in Fig. 4. One could see that both pure Ag₂C₂O₄ and P25-TiO₂ only absorb ultraviolet light in association with the absorption-edge locating at about 324 nm and 390 nm, respectively. The absorption edge of the sample can be determined from the following equation:

$$E_g = 1239.8/\lambda \quad (1)$$

Where E_g is the band gap (eV) and λ (nm) is the optical absorption edge. Namely, the band gap energies of Ag₂C₂O₄ and P25-TiO₂ could be calculated for 3.83 eV and 3.18 eV, respectively, both of which belong to wide band gap semiconductors.

The valence band (VB) edge position of Ag₂C₂O₄ was estimated according to the concept of electronegativity [8,32,33]. The con-

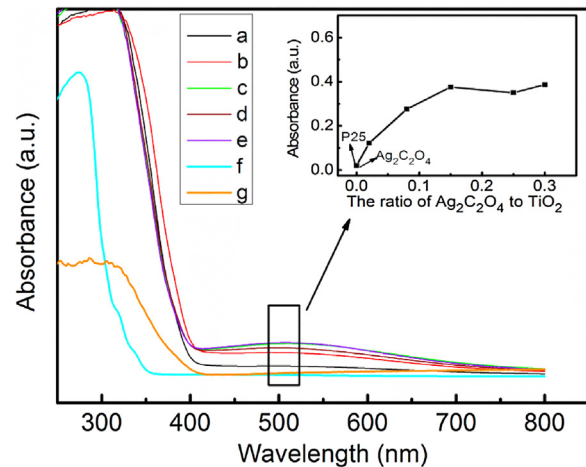


Fig. 4. UV-vis diffuse reflectance spectra of $\text{Ag}_2\text{C}_2\text{O}_4$, P25-TiO₂ and $\text{Ag}_2\text{C}_2\text{O}_4/\text{TiO}_2$ composite samples: (a) $\text{Ag}_2\text{C}_2\text{O}_4/\text{TiO}_2$ -0.02, (b) $\text{Ag}_2\text{C}_2\text{O}_4/\text{TiO}_2$ -0.08, (c) $\text{Ag}_2\text{C}_2\text{O}_4/\text{TiO}_2$ -0.15, (d) $\text{Ag}_2\text{C}_2\text{O}_4/\text{TiO}_2$ -0.25, (e) $\text{Ag}_2\text{C}_2\text{O}_4/\text{TiO}_2$ -0.3, (f) $\text{Ag}_2\text{C}_2\text{O}_4$, (g) P25 TiO₂. Inset: change of visible light absorptivity at 500 nm with the ratio of $\text{Ag}_2\text{C}_2\text{O}_4$ to TiO₂.

duction band (CB) and VB potentials of Ag₂C₂O₄ at the point of zero charge can be calculated by the following equation:

$$E_{\text{VB}} = X - E^{\text{e}} + 0.5E_g \quad (2)$$

Where E_{VB} is the valence band edge potential; E^{e} is the energy of free electrons on the hydrogen scale (ca. 4.5 eV); and E_g is the band gap of the Ag₂C₂O₄ that have been calculated as 3.83 eV; X is the absolute electronegativity of the semiconductor, which is defined as the geometric mean of the absolute electronegativity of the constituent atoms by the following equation [34]:

$$X = (x_1^r \cdot x_2^s \cdots x_{n-1}^p \cdot x_n^q)^{1/N} \quad (3)$$

where x_n is the electronegativity of the constituent atom; n is the number of the species; N is the total number of atoms in the compound; The superscripts r , s , p , ..., q refer to the numbers of the atoms 1, 2, ..., $n-1$ and n , respectively in the molecule, so that $r+s+\dots+p+q=N$. The x values of Ag, C and O are 4.44, 6.27 and 7.54 eV, respectively [35]. According to equation 2 and 3, the values of X and E_{VB} for Ag₂C₂O₄ are calculated to be 6.31 and 3.72 eV. The conduction band position can be determined to be -0.11 eV by $E_{\text{CB}} = E_{\text{VB}} - E_g$.

In case of Ag₂C₂O₄/TiO₂ nanocomposites, the absorption extends from UV to visible light region and shows stronger absorption around 450–650 nm. The inset in Fig. 4 displays the absorptivity at 500 nm as a function of the weight ratio of Ag₂C₂O₄

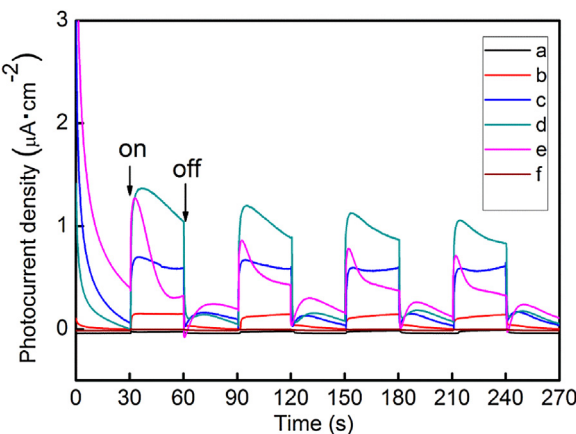


Fig. 5. Transient photocurrent responses of different electrodes under visible light irradiation: (a) $\text{Ag}_2\text{C}_2\text{O}_4/\text{TiO}_2$ -0.02, (b) $\text{Ag}_2\text{C}_2\text{O}_4/\text{TiO}_2$ -0.08, (c) $\text{Ag}_2\text{C}_2\text{O}_4/\text{TiO}_2$ -0.15, (d) $\text{Ag}_2\text{C}_2\text{O}_4/\text{TiO}_2$ -0.25, (e) $\text{Ag}_2\text{C}_2\text{O}_4/\text{TiO}_2$ -0.3, (f) P25-TiO₂.

to TiO₂. It initially increases with increasing the weight ratio and then reaches a nearly steady value. Considering the preparation and DRS measurement method, two factors can be ascribed to the visible light absorption. One is that there probably formed $\text{Ag}_2\text{C}_2\text{O}_4/\text{TiO}_2$ heterojunction resulting in quantum effect beneficial to the visible light absorption. Another probably reason could be ascribed to the surface plasmon resonance effect of Ag nanoparticles that derived from mechanical grinding in quartz bowl before DRS measurement. Some reporters have been found that Ag oxalate could be decomposed into Ag nanoparticles by mechanochemical method even simple collisions [36–38]. Therefore, it can be inferred that a handful of Ag formed on the surface of $\text{Ag}_2\text{C}_2\text{O}_4/\text{TiO}_2$ nanocomposites due to the grinding effect. Moreover, the characteristic absorption of the surface plasmon resonance effect of Ag nanoparticles is just lying in the range of 450–700 [39–41], well accordance with the above results.

3.4. Transient photocurrent response

Transient photocurrent responses were determined to investigate the charge separation and migration of photocatalysts. Fig. 5 demonstrates the comparison of photocurrent responses of different samples conducted under intermittent visible light irradiation. There were no photocurrent responses for P25-TiO₂ possibly due to the wide band gap. As for $\text{Ag}_2\text{C}_2\text{O}_4/\text{TiO}_2$ nanocomposites, one could see that the photocurrent rises rapidly to a constant value when the light was turned on, while the photocurrent immediately decreases to nearly zero as long as the light was off. It can be seen from Fig. 5 that photocurrent density were reproducible during the repeated

on-off cycles under visible light irradiation, indicating photocatalysts were stable under the illumination [42]. There appears an anodic photocurrent peak at the initial time of irradiation followed gradually decay until light-off. When the light is switched off, a cathodic peak can also be observed. The initial current can be attributed to the separation of electron-hole pairs at the photocatalysts/electrolyte interface. The decay of the photocurrent indicates that a fraction of the holes reaching the semiconductor surface, instead of capturing electrons from the electrolyte, either recombine with electrons from the conduction band and/or accumulate at the surface [33]. When the light is switched off, the holes accumulated in the surface still continue to recombine, resulting in the cathodic peak. The above results indicates that there may be exist some grain boundaries in the direction of electron diffusion [43], very possibly originated from the $\text{Ag}_2\text{C}_2\text{O}_4/\text{TiO}_2$ heterojunction [9,13,14,24]. $\text{Ag}_2\text{C}_2\text{O}_4/\text{TiO}_2$ -0.02 showed nearly no photocurrent responses, which can be ascribed to the trace $\text{Ag}_2\text{C}_2\text{O}_4$ incorporation well in accordance to the optical absorption results. With the increase of $\text{Ag}_2\text{C}_2\text{O}_4$ weight ratio, the photocurrent density initially increases from 0.15 mA cm^{-2} for $\text{Ag}_2\text{C}_2\text{O}_4/\text{TiO}_2$ -0.08 to a maximum value of 1.38 mA cm^{-2} for $\text{Ag}_2\text{C}_2\text{O}_4/\text{TiO}_2$ -0.25, respectively. Further increase in the $\text{Ag}_2\text{C}_2\text{O}_4$ weight ratio up to 0.3 leads to a decrease in photocurrent density from 1.38 mA cm^{-2} to 0.85 mA cm^{-2} (for $\text{Ag}_2\text{C}_2\text{O}_4/\text{TiO}_2$ -0.30). Moreover, the photocurrent of $\text{Ag}_2\text{C}_2\text{O}_4/\text{TiO}_2$ -0.3 was terribly unstable, indicating that more $\text{Ag}_2\text{C}_2\text{O}_4$ incorporated into P25-TiO₂ was not benefit to the charge separation and migration, well accordance with its photocatalytic performance.

3.5. Visible light photocatalytic performance

The experiment of propylene degradation was measured in system I, equipped with a gas chromatograph for *in-situ* analysis. Prior to irradiation, the feed gas was flowing continuously until the propylene adsorption-desorption equilibrium was established. Fig. 6 shows the photocatalytic degradation of propylene over P25-TiO₂, $\text{Ag}_2\text{C}_2\text{O}_4$ and $\text{Ag}_2\text{C}_2\text{O}_4/\text{TiO}_2$ nanocomposites and CO₂ production under visible light irradiation. The propylene removal rate over P25-TiO₂ is only 8% (see Fig. 6A) under visible light irradiation, corresponding to inertness of P25-TiO₂ with a large band gap towards visible light photocatalytic oxidation of propylene. Contrary to the above, propylene is photodegraded as soon as the light is turned on, and the maximum removal rate of propylene over $\text{Ag}_2\text{C}_2\text{O}_4$ is up to ca. 52.7%, even $\text{Ag}_2\text{C}_2\text{O}_4$ possessing wider band gap than P25-TiO₂. Unfortunately, the visible light photocatalytic activity of $\text{Ag}_2\text{C}_2\text{O}_4$ gradually declines with extending reaction time. This indicates that $\text{Ag}_2\text{C}_2\text{O}_4$ is unstable possibly due to photo-corrosion under visible light irradiation, which can be confirmed by the CO₂ production results. As can be seen from Fig. 6B,

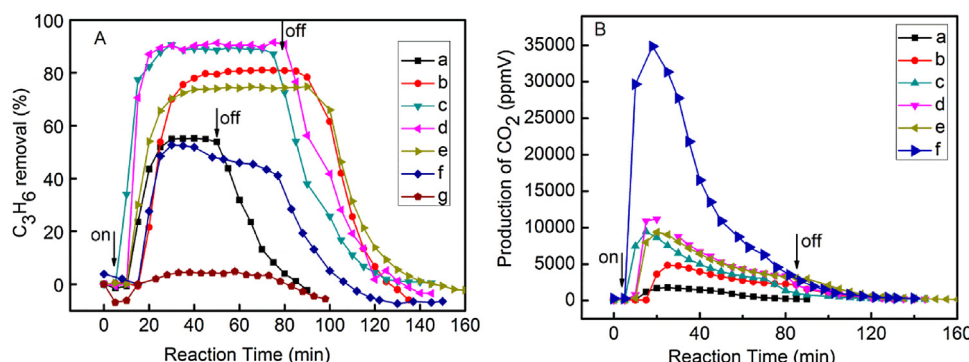


Fig. 6. Visible light photoactivity of P25, $\text{Ag}_2\text{C}_2\text{O}_4$ and $\text{Ag}_2\text{C}_2\text{O}_4/\text{TiO}_2$ composites evaluated by C_3H_6 removal (vol%) (A); Change of CO₂ production with irradiation time (B). (a) $\text{Ag}_2\text{C}_2\text{O}_4/\text{TiO}_2$ -0.02, (b) $\text{Ag}_2\text{C}_2\text{O}_4/\text{TiO}_2$ -0.08, (c) $\text{Ag}_2\text{C}_2\text{O}_4/\text{TiO}_2$ -0.15, (d) $\text{Ag}_2\text{C}_2\text{O}_4/\text{TiO}_2$ -0.25, (e) $\text{Ag}_2\text{C}_2\text{O}_4/\text{TiO}_2$ -0.3, (f) $\text{Ag}_2\text{C}_2\text{O}_4$, (g) P25-TiO₂.

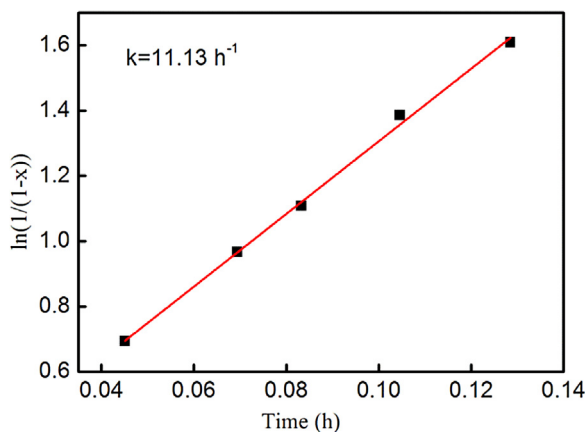


Fig. 7. The first-order kinetic for degradation of propylene by $\text{Ag}_2\text{C}_2\text{O}_4/\text{TiO}_2$ -0.25 under visible light irradiation.

a CO_2 concentration spike with a value of 34711 ppmV, which immediately declined continuously, appears at the initial time of irradiation over $\text{Ag}_2\text{C}_2\text{O}_4$. Noticing that 3 mol CO_2 should be generated by complete oxidation of 1 mol of C_3H_6 , the obtained CO_2 concentration is far more than that of complete oxidation of propylene ($500 \text{ ppm} \times 52.7\% \times 3 = 795 \text{ ppm}$). It can be inferred that there must have other sources of CO_2 . Considering that Ag-based photocatalysts usually experience photo-corrosion under visible light irradiation, the extra more CO_2 content should be derived from the photo-corrosion of $\text{Ag}_2\text{C}_2\text{O}_4$ as follow:



With extending the irradiation time, the nascent metallic Ag generated on the surface of substrate $\text{Ag}_2\text{C}_2\text{O}_4$ should hinder the photo-corrosion happening. Therefore, the gradual decay of CO_2 concentration was observed and a plasmonic photocatalyst $\text{Ag}@\text{Ag}_2\text{C}_2\text{O}_4$ formed thereby [44], accounting for the unstable visible light photocatalytic performance.

Differently from the instability of $\text{Ag}_2\text{C}_2\text{O}_4$, all the resultant $\text{Ag}_2\text{C}_2\text{O}_4/\text{TiO}_2$ nanocomposites exhibit highly efficient and stable visible light photocatalytic activity after $\text{Ag}_2\text{C}_2\text{O}_4$ incorporation with P25-TiO₂ (see Fig. 6A). This means that combination with P25-TiO₂ helps to efficiently utilize the photo-corrosion of $\text{Ag}_2\text{C}_2\text{O}_4$ thereby leading to greatly increased photocatalytic activity and stability of $\text{Ag}_2\text{C}_2\text{O}_4/\text{TiO}_2$ under visible light irradiation, which possibly because the surface plasmon resonance of Ag derived from the photo-corrosion of $\text{Ag}_2\text{C}_2\text{O}_4$ as discussed in detail below. With increase the weight ratio of $\text{Ag}_2\text{C}_2\text{O}_4$, the removal rate of propylene enhanced from 55% for $\text{Ag}_2\text{C}_2\text{O}_4/\text{TiO}_2$ -0.02 to 91% for $\text{Ag}_2\text{C}_2\text{O}_4/\text{TiO}_2$ -0.25 followed by decline to 74% for $\text{Ag}_2\text{C}_2\text{O}_4/\text{TiO}_2$ -

0.3, respectively. In the case of $\text{Ag}_2\text{C}_2\text{O}_4/\text{TiO}_2$ -0.25, the best photocatalytic behavior can be ascribed to the optimized optical absorption and transient photocurrent response.

Fig. 6B shows the change of CO_2 production with irradiation time. It can be seen that the change trends of CO_2 production over all $\text{Ag}_2\text{C}_2\text{O}_4/\text{TiO}_2$ composites are similar to that of pure $\text{Ag}_2\text{C}_2\text{O}_4$. As light is turned on, the produced CO_2 first sharply reaches the maximum, and then gradually decreases to a steady value. Moreover, the amount of produced CO_2 is related with not only the activity of catalyst but also the content of $\text{Ag}_2\text{C}_2\text{O}_4$ in $\text{Ag}_2\text{C}_2\text{O}_4/\text{TiO}_2$ composites. This indicates that photodecomposition of $\text{Ag}_2\text{C}_2\text{O}_4$ in $\text{Ag}_2\text{C}_2\text{O}_4/\text{TiO}_2$ composites also happened under visible light.

The kinetic behavior of $\text{Ag}_2\text{C}_2\text{O}_4/\text{TiO}_2$ nanocomposites in degradation of propylene were measured and analyzed. $\text{Ag}_2\text{C}_2\text{O}_4/\text{TiO}_2$ -0.25 photocatalyst was selected as representative sample to evaluate the photocatalytic activities under different flow rate of the feed gas. As the flow rate was adjusted to 554, 360, 300, 239 and 194.6 mL h^{-1} , respectively, the removal rate of propylene was tested to be 50%, 62%, 67%, 75% and 80% accordingly. Assuming that the propylene degradation follows the first-order kinetics, the equation $\ln [1/(1-x)] = kt$ will be applied, where x is the removal rate of propylene, k is the reaction rate constant and t is the irradiation time. In this photocatalytic reaction system (i.e. system I), dividing the irradiated photo-reactor volume (25 mL) by the flow rate of the feed gas to get the irradiation time t. For example, the reaction time t equals to 0.0451 h when the flow rate is 554 mL h^{-1} ($t = 25 \text{ mL}/554 \text{ mL h}^{-1}$). The curve of $\ln [1/(1-x)]$ vs. irradiation time t is shown in Fig. 7. It can be seen that the value of linear correlation coefficient R for $\text{Ag}_2\text{C}_2\text{O}_4/\text{TiO}_2$ -0.25 is 0.9984, confirming the first order trend of degradation of propylene by $\text{Ag}_2\text{C}_2\text{O}_4/\text{TiO}_2$ catalyst. Moreover, the reaction rate constant of $\text{Ag}_2\text{C}_2\text{O}_4/\text{TiO}_2$ -0.25 was calculated to be 11.13 h^{-1} . The results demonstrate that $\text{Ag}_2\text{C}_2\text{O}_4/\text{TiO}_2$ -0.25 can be used as highly efficient photocatalyst for degradation of propylene under visible light.

The degradations of acetaldehyde gas over $\text{Ag}_2\text{C}_2\text{O}_4/\text{TiO}_2$ nanocomposites, P25-TiO₂ and $\text{Ag}_2\text{C}_2\text{O}_4$ were also tested under visible light irradiation in system II. All of the degradation was carried out after the dark adsorption equilibrium. As shown in Fig. 8a. TiO₂ exhibits nearly no activity in this experiment. And the $\text{Ag}_2\text{C}_2\text{O}_4/\text{TiO}_2$ composite exhibits much higher activity than pure $\text{Ag}_2\text{C}_2\text{O}_4$. The linear relationship between $\ln (C_0/C)$ and irradiation time are shown in Fig. 8b. The reaction rate constant k and linear correlation coefficient R for $\text{Ag}_2\text{C}_2\text{O}_4/\text{TiO}_2$ composite with different weight ratio of $\text{Ag}_2\text{C}_2\text{O}_4$ to TiO_2 in degrading acetaldehyde gas are summarized in Table 1. The values of R for all the cases were higher than 0.97, confirming the first order nature of the degradation of acetaldehyde by $\text{Ag}_2\text{C}_2\text{O}_4/\text{TiO}_2$ composites. The rate constant k of $\text{Ag}_2\text{C}_2\text{O}_4/\text{TiO}_2$ composite is in the order of $\text{Ag}_2\text{C}_2\text{O}_4/\text{TiO}_2$ -0.25 > $\text{Ag}_2\text{C}_2\text{O}_4/\text{TiO}_2$ -0.08 > $\text{Ag}_2\text{C}_2\text{O}_4/\text{TiO}_2$ -

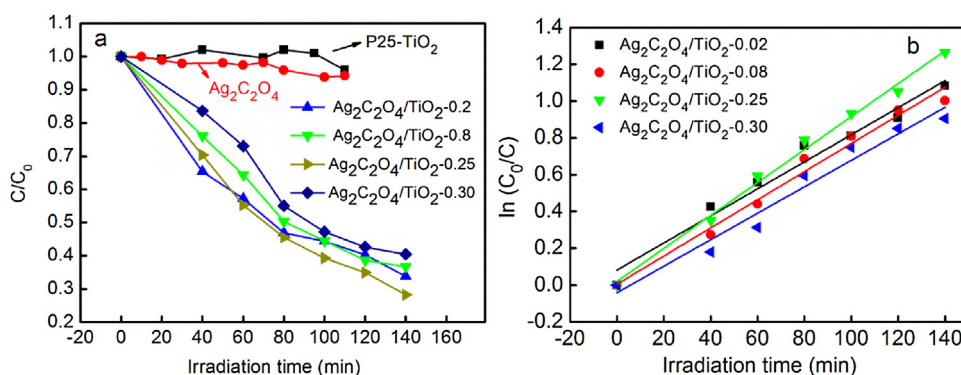


Fig. 8. Degradation of acetaldehyde (a) and the first order kinetic (b) over different catalyst under visible light irradiation.

Table 1

The reaction rate constant k and correlation coefficient R for $\text{Ag}_2\text{C}_2\text{O}_4/\text{TiO}_2$ composite with different weight ratio of $\text{Ag}_2\text{C}_2\text{O}_4$ to TiO_2 in degrading acetaldehyde test under visible light irradiation.

Catalyst	Weight ratio of $\text{Ag}_2\text{C}_2\text{O}_4$ to TiO_2	Correlation coefficient R	Reaction rate constant k (min^{-1}) for the degradation of acetaldehyde
$\text{Ag}_2\text{C}_2\text{O}_4/\text{TiO}_2\text{-}0.02$	0.02:1	0.983	0.00735
$\text{Ag}_2\text{C}_2\text{O}_4/\text{TiO}_2\text{-}0.08$	0.08:1	0.989	0.00764
$\text{Ag}_2\text{C}_2\text{O}_4/\text{TiO}_2\text{-}0.25$	0.25:1	0.996	0.00896
$\text{Ag}_2\text{C}_2\text{O}_4/\text{TiO}_2\text{-}0.3$	0.30:1	0.979	0.00719

0.02 > $\text{Ag}_2\text{C}_2\text{O}_4/\text{TiO}_2\text{-}0.3$, indicating that, similar to the oxidation of propylene, $\text{Ag}_2\text{C}_2\text{O}_4/\text{TiO}_2\text{-}0.25$ catalyst still shows the highest activity for the degradation of acetaldehyde.

As many literatures reported, silver-based semiconductor photocatalysts are easy to decrease their photocatalytic activity due to the photocorrosion. Yu et al. found that Ag_2CO_3 almost lose its activity in the second run of the recycling reaction for the degradation of methyl orange [19]. Fa et al. reported that the photocatalytic degradation ability of $\text{Ag}_3\text{PO}_4/\text{Ag}_2\text{CO}_3$ photocatalyst continuously decreased with increase cycling runs possibly due to the decomposition of Ag_3PO_4 and Ag_2CO_3 into metallic silver [45]. Wang et al. revealed that both $\text{AgBr}/\text{Ag}_3\text{PO}_4$ and $\text{AgBr}/\text{Ag}_3\text{PO}_4/\text{TiO}_2$ showed apparent downturn activity in successive MO degradation runs [46]. To compare the stability between pure $\text{Ag}_2\text{C}_2\text{O}_4$ and $\text{Ag}_2\text{C}_2\text{O}_4/\text{TiO}_2\text{-}0.25$ nanocomposite photocatalyst, recycle experiments of propylene degradation in association with CO_2 production were carried out. As shown in Fig. 9a, it can be seen that the visible light photocatalytic activity over pure $\text{Ag}_2\text{C}_2\text{O}_4$ slightly decreased from 52.7% to 40.6% after four cycles. In the first run, as discussed above, pure $\text{Ag}_2\text{C}_2\text{O}_4$ experienced photo-corrosion in the process of propylene degradation and a CO_2 concentration spike with the value of 34711 ppmV appeared as long as the light on, which immediately declined continuously until the light off. However, the CO_2 concentration spike surprisingly disappeared from the second to fourth cycling run. Combined with above two results, it can be inferred that the photo-corrosion was almost complete in the first cycle and most of carbon dioxide detected resulted from the decom-

position of $\text{Ag}_2\text{C}_2\text{O}_4$. Furthermore, the CO_2 concentration platform should be almost derived from the photodegradation of propylene with regard to the second to fourth cycling run. Contrary to pure $\text{Ag}_2\text{C}_2\text{O}_4$, $\text{Ag}_2\text{C}_2\text{O}_4/\text{TiO}_2\text{-}0.25$ possessed highly stable visible light photocatalytic activity in four successive cycling runs (see Fig. 9c). However, similar to pure $\text{Ag}_2\text{C}_2\text{O}_4$, a CO_2 concentration spike with the value of 17531 ppmV also initially appeared as long as the light on and immediately declined continuously until the light off for $\text{Ag}_2\text{C}_2\text{O}_4/\text{TiO}_2\text{-}0.25$. It means that both pure $\text{Ag}_2\text{C}_2\text{O}_4$ and $\text{Ag}_2\text{C}_2\text{O}_4/\text{TiO}_2\text{-}0.25$ nanocomposite underwent the same photo-corrosion process.

To reveal the relation between the photo-decomposition of $\text{Ag}_2\text{C}_2\text{O}_4$ and the activity of $\text{Ag}_2\text{C}_2\text{O}_4$ as well as $\text{Ag}_2\text{C}_2\text{O}_4/\text{TiO}_2$, we further conducted SEM, TEM, XPS and XRD analysis of $\text{Ag}_2\text{C}_2\text{O}_4$ and $\text{Ag}_2\text{C}_2\text{O}_4/\text{TiO}_2\text{-}0.25$ after visible light irradiation. It can be observed from Fig. 10a that an obvious hole inserted with several particles is present on a smooth surface of $\text{Ag}_2\text{C}_2\text{O}_4$, and many raised circular particles are also distributed on the other surface. It is clear that pristine $\text{Ag}_2\text{C}_2\text{O}_4$ underwent the photodecomposition introducing silver particles and CO_2 gas during visible light irradiation. Fig. 10b is the TEM image of $\text{Ag}_2\text{C}_2\text{O}_4/\text{TiO}_2\text{-}0.25$ composite after visible light irradiation. There is no obvious change can be seen from the image comparison between before (Fig. 10c) and after irradiation. This may be resulted from the particle size of adhered $\text{Ag}_2\text{C}_2\text{O}_4$ or Ag, which is too small to distinguish. However, from Ag Auger MVV spectra of $\text{Ag}_2\text{C}_2\text{O}_4$ (Fig. 11a) and $\text{Ag}_2\text{C}_2\text{O}_4/\text{TiO}_2\text{-}0.25$ (Fig. 11b) before and after irradiation, it is seen that the peak at

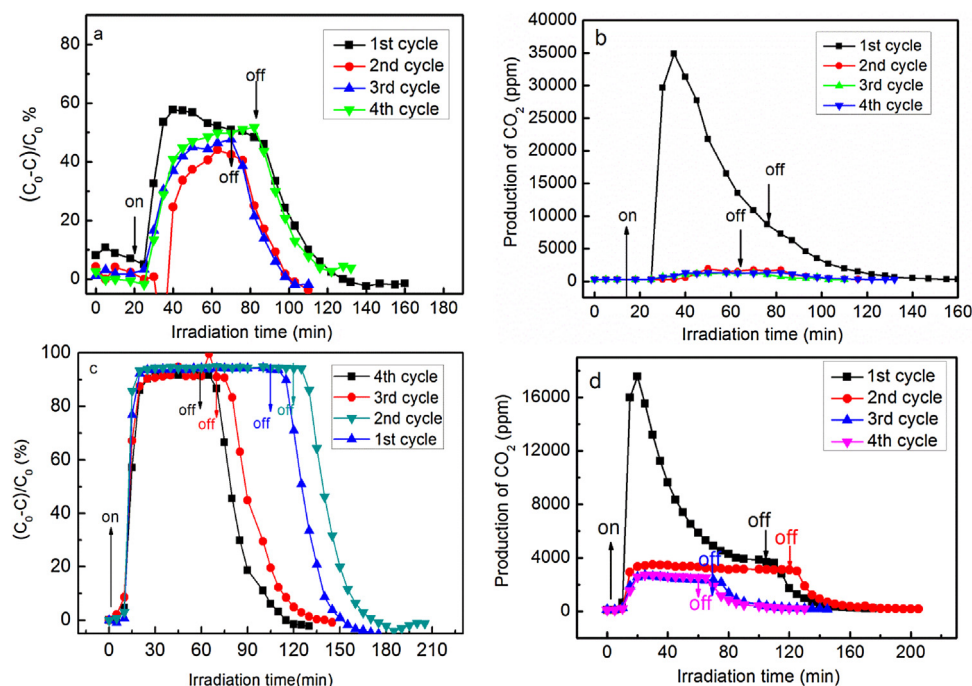


Fig. 9. Repetitive degradations of propylene over pure $\text{Ag}_2\text{C}_2\text{O}_4$ (a) and $\text{Ag}_2\text{C}_2\text{O}_4/\text{TiO}_2\text{-}0.25$ composite (c) as well as recycling change of CO_2 production with irradiation time over $\text{Ag}_2\text{C}_2\text{O}_4$ (b) and $\text{Ag}_2\text{C}_2\text{O}_4/\text{TiO}_2\text{-}0.25$ (d) under visible light irradiation.

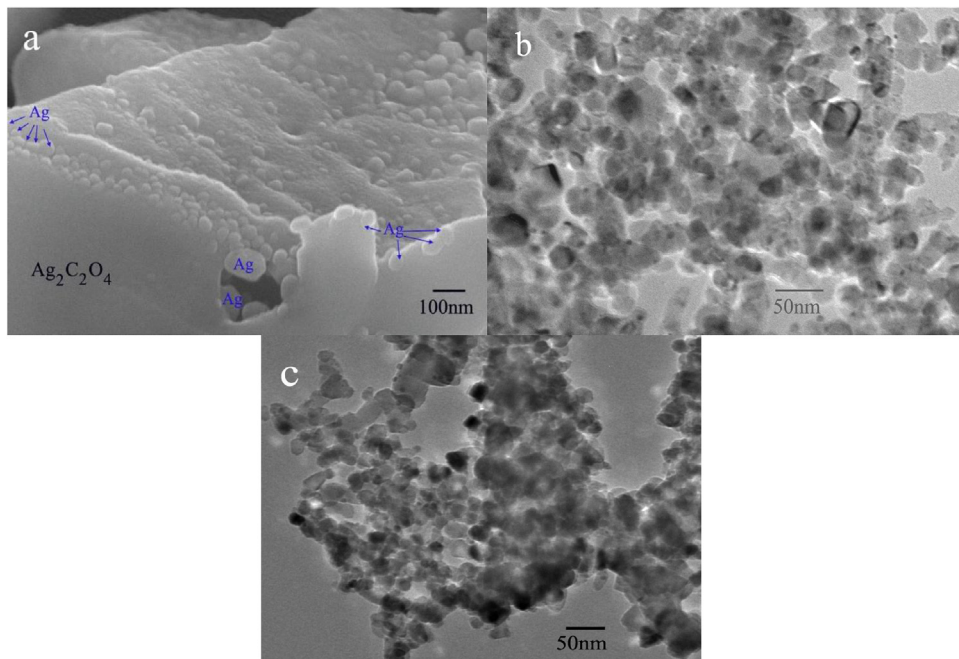


Fig. 10. SEM image of $\text{Ag}_2\text{C}_2\text{O}_4$ after irradiation (a) as well as TEM image of $\text{Ag}_2\text{C}_2\text{O}_4/\text{TiO}_2\text{-}0.25$ after (b) and before (c) irradiation.

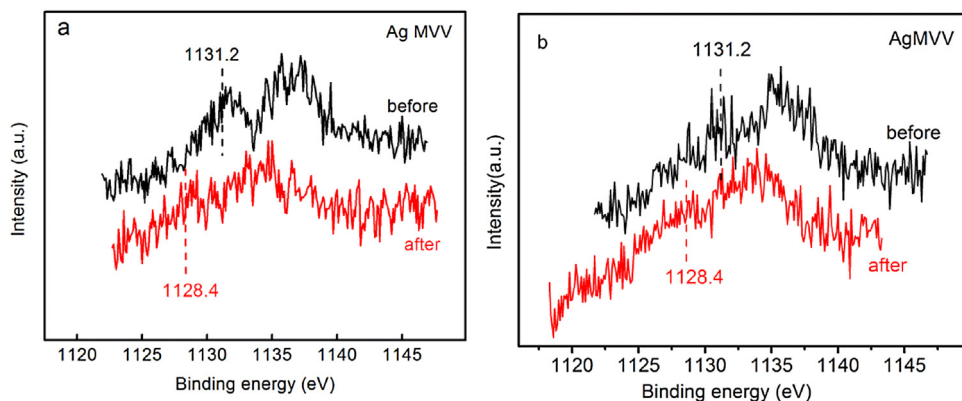


Fig. 11. Auger Ag MVV XPS spectra of as-prepared $\text{Ag}_2\text{C}_2\text{O}_4$ (a) and $\text{Ag}_2\text{C}_2\text{O}_4/\text{TiO}_2\text{-}0.25$ (b) before and after visible light irradiation.

1131.2 eV largely shifted to 1128.6 eV after four-cycle propylene photodegradation experiments for both samples. This indicates that partial Ag^+ in $\text{Ag}_2\text{C}_2\text{O}_4$ and $\text{Ag}_2\text{C}_2\text{O}_4/\text{TiO}_2\text{-}0.25$ were reduced to Ag [26], confirming again that the photo-corrosion happened during photocatalytic process. Furthermore, Fig. 12a shows XRD

patterns comparison of $\text{Ag}_2\text{C}_2\text{O}_4$ before and after irradiation. It can be seen that, after recycle experiments, the typical characteristic peaks of Ag at 38.2° , 44.2° , 64.4° , and 77.4° clearly appeared in addition to the diffraction peaks of $\text{Ag}_2\text{C}_2\text{O}_4$ [47,48], which is well consistent with XPS results. It demonstrated that during

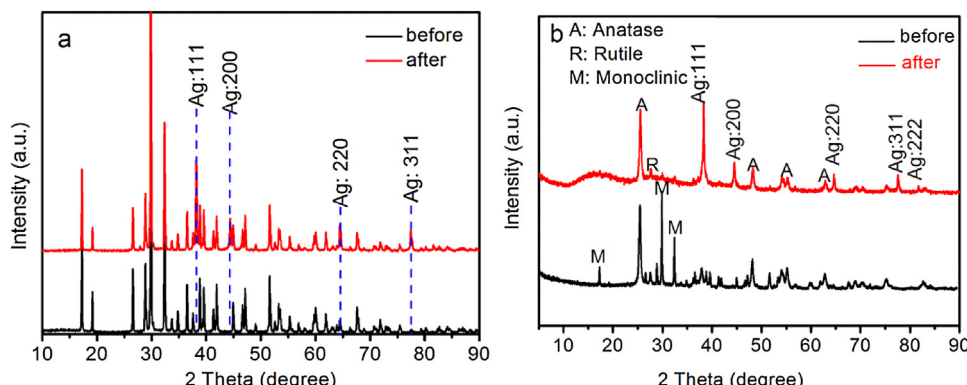


Fig. 12. XRD patterns of as-prepared $\text{Ag}_2\text{C}_2\text{O}_4$ (a) and $\text{Ag}_2\text{C}_2\text{O}_4/\text{TiO}_2\text{-}0.25$ (b) before and after visible light irradiation.

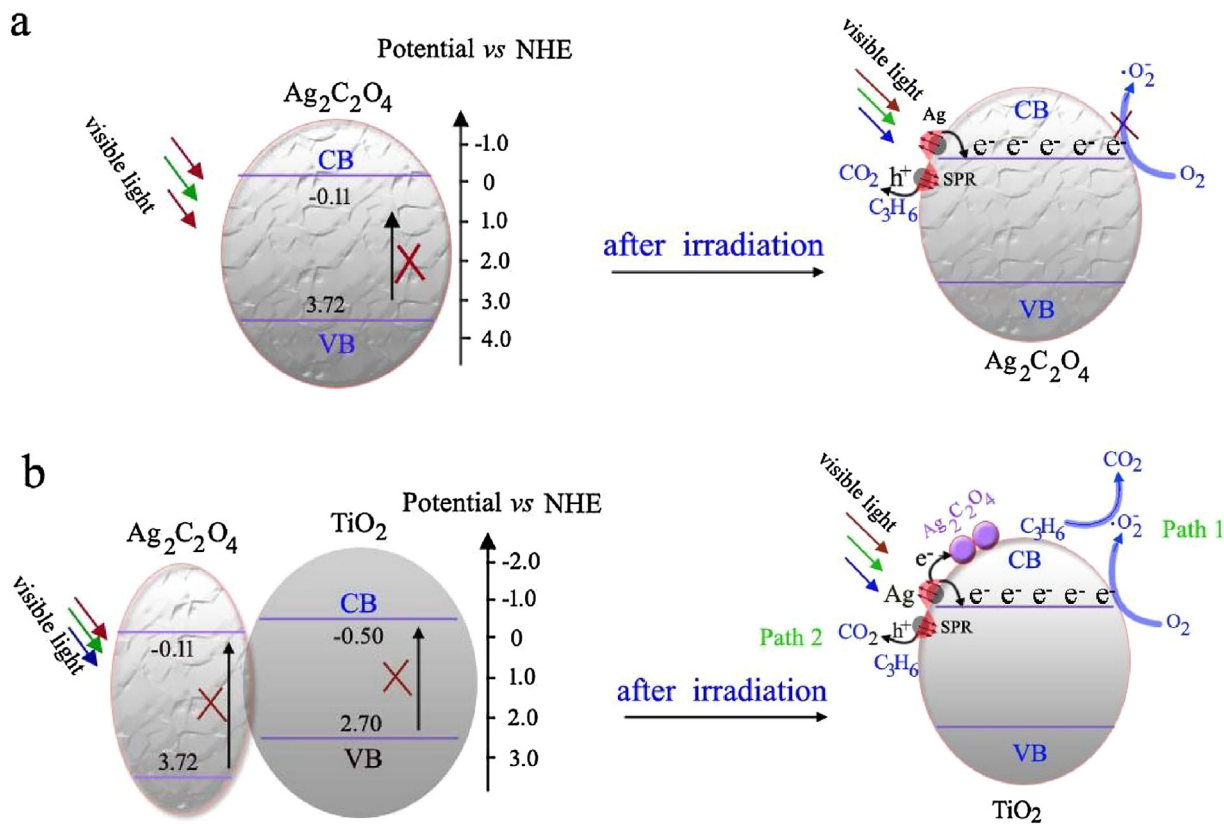


Fig. 13. Photocatalytic mechanism diagrams of Ag₂C₂O₄ (a) and Ag₂C₂O₄/TiO₂-0.25 (b).

photocatalytic process, wide-band-gap Ag₂C₂O₄ semiconductor is gradually changed into Ag@Ag₂C₂O₄ composites. Similarly, as for Ag₂C₂O₄/TiO₂-0.25, after successive four-cycle experiments, the intensity of characteristic diffraction peaks of Ag₂C₂O₄ dramatically decrease and the cubic Ag is demonstrated to be formed with five intense peaks at 38.2°, 44.2°, 64.4°, 77.4°, and 80.7°, which can be assigned to (111), (200), (220), (311) and (222) lattice planes. This, in combination with XPS results, indicates that Ag₂C₂O₄/TiO₂-0.25 has transformed into a new photocatalyst Ag@Ag₂C₂O₄/TiO₂ during visible light irradiation process.

3.6. Photocatalytic mechanism of Ag₂C₂O₄ and Ag₂C₂O₄/TiO₂ under visible light irradiation

It seems impossible for Ag₂C₂O₄ or Ag₂C₂O₄/TiO₂ to show visible light activity due to its wide band gap. Surprisingly, the photo-corrosion of Ag₂C₂O₄ happened during photocatalytic process affording nascent metallic Ag and a plasmonic photocatalyst Ag@Ag₂C₂O₄ or Ag@Ag₂C₂O₄/TiO₂ formed thereby. It can be expected that the nascent metallic Ag scattered in situ on the substrate Ag₂C₂O₄ or P25-TiO₂. As we all know, the plasma resonance effect of noble metals such as Au and Ag can be used to promote the photocatalytic performance [49]. Namely, on the one hand, if semiconductor can be excited to generate e⁻ – h⁺ pair by visible light, Ag will effectively trap the photogenerated e⁻ and transfer to adsorbed oxygen to produce reactive oxygen species O₂⁻ radicals. Kuai et al. successfully fabricate a stable and highly efficient direct sunlight plasmonic photocatalyst Ag-AgBr through a facile hydrothermal [50]. It was found that the produced Ag nanoparticles not only prevent the decomposition of AgBr but also suppress the recombination of e⁻ and h⁺. On the other hand, silver nanoparticles can also be excited by visible light to generate e⁻ and h⁺ due to the plasma resonance effect. Many studies have reported that

the excited electrons from noble metals, such as Au and Ag, can also be injected into the conduction band (CB) of TiO₂ to react with adsorbed oxygen forming superoxide radicals [51–53]. The visible light photocatalytic mechanisms over Ag₂C₂O₄ and Ag₂C₂O₄/TiO₂ are proposed. As shown in Fig. 13a, the plasma-excited holes from the surface of Ag could oxidize the organics into CO₂ [50,54,55] and the plasma-excited electrons could transfer to the conduction band of Ag₂C₂O₄ because of the more positive CB energy of Ag₂C₂O₄ (-0.11 eV) than that of TiO₂ (-0.50 eV). However, the electrons transferred to CB of Ag₂C₂O₄ cannot react with adsorbed O₂ due to the lower potential of CB (-0.11) than that of O₂/O₂⁻ (-0.33) [56]. As for Ag@Ag₂C₂O₄/TiO₂ (Fig. 13b) evolved from Ag₂C₂O₄/TiO₂, besides the excited h⁺ for the oxidation of organics, the excited electrons transferred to the CB of TiO₂ can be applied to produce reactive oxide radicals O₂⁻ due to the more negative potential (-0.50 eV) than that of O₂/O₂⁻ (-0.33). Two degradation paths make the visible-light-activity of Ag₂C₂O₄/TiO₂ to be much higher than that of Ag₂C₂O₄. Furthermore, the size and loading amount of the silver nanoparticles strongly affect the photocatalytic performance of the plasmonic photocatalyst Ag@Ag₂C₂O₄/TiO₂. Tian et al. have reported that interfacial electron transfer process depends on the size of noble metals on TiO₂ surface [57]. When the size of gold particles is too large, the Fermi energy level of gold particles will be lower than the conduction band edge of TiO₂ and hence the generated electrons from TiO₂ can be captured by Au particles. However, for quantum sized gold particles, the excited electrons can transfer to the conduction band of TiO₂ from gold particles since its Fermi energy level is higher than TiO₂ CB edge. In the present work, the size of Ag particles of Ag@Ag₂C₂O₄/TiO₂ (see Fig. 10b) is about 1–5 nm, which is much smaller than that of Ag particles on the surface of Ag₂C₂O₄ (see Fig. 10a). This may be another factor that Ag₂C₂O₄/TiO₂ exhibited more superior photocatalytic performance than that of Ag₂C₂O₄.

4. Conclusions

In summary, pure $\text{Ag}_2\text{C}_2\text{O}_4$ and $\text{Ag}_2\text{C}_2\text{O}_4/\text{TiO}_2$ nanocomposite photocatalysts have been synthesized by a facial liquid precipitation method. The visible-light activity and the kinetic behavior of $\text{Ag}_2\text{C}_2\text{O}_4$ and $\text{Ag}_2\text{C}_2\text{O}_4/\text{TiO}_2$ have also been evaluated by the degradation of propylene and acetaldehyde gas. Compared to pure $\text{Ag}_2\text{C}_2\text{O}_4$ and $\text{P}25\text{-TiO}_2$, $\text{Ag}_2\text{C}_2\text{O}_4/\text{TiO}_2$ exhibited much higher visible light activity and its kinetic behavior was accordant with the first order reaction formula for the degradation of propylene and acetaldehyde. The comparison of SEM, TEM, XPS and XRD results between before and after visible light photocatalytic reaction demonstrated that both $\text{Ag}_2\text{C}_2\text{O}_4$ and $\text{Ag}_2\text{C}_2\text{O}_4/\text{TiO}_2$ experienced the photo-decomposition generating nascent metallic Ag during photocatalytic process. The nascent metallic Ag was expected to scatter *in situ* on the substrate $\text{Ag}_2\text{C}_2\text{O}_4$ or $\text{P}25\text{-TiO}_2$, forming the plasmonic photocatalyst $\text{Ag@Ag}_2\text{C}_2\text{O}_4$ or $\text{Ag@Ag}_2\text{C}_2\text{O}_4/\text{TiO}_2$. The mechanism of highly efficient and stable photocatalytic activity was proposed. On the one hand, $\text{Ag}_2\text{C}_2\text{O}_4$ undergoes firstly photo-corrosion during the initial photocatalytic process generating nascent metallic Ag on the surface of $\text{Ag}_2\text{C}_2\text{O}_4$, which subsequently endowing the $\text{Ag@Ag}_2\text{C}_2\text{O}_4$ with visible light photocatalytic activity due to the plasma resonance of Ag. On the other hand, $\text{Ag}_2\text{C}_2\text{O}_4/\text{TiO}_2$ nanocomposites also experience the same journey resulting in the formation of $\text{Ag@Ag}_2\text{C}_2\text{O}_4/\text{TiO}_2$. Differently from $\text{Ag@Ag}_2\text{C}_2\text{O}_4$, two paths are involved to separate the electron and hole excited by the photon of nascent metallic Ag so as to acquire much higher photocatalytic activity for $\text{Ag@Ag}_2\text{C}_2\text{O}_4/\text{TiO}_2$.

Acknowledgement

The authors acknowledge the financial support provided by the Science and Technology Research Project of Henan province (Grant No. 15A150040, 162102210178, 18A150022).

References

- [1] P. Wang, B. Huang, X. Qin, X. Zhang, Y. Dai, J. Wei, M.H. Whangbo, *Angew. Chem. Int. Ed.* 47 (2008) 7931–7933.
- [2] S. Ouyang, N. Kikugawa, D. Chen, Z. Zou, J. Ye, *J. Phys. Chem. C* 113 (2009) 1560–1566.
- [3] J. Singh, S. Uma, *J. Phys. Chem. C* 113 (2009) 12483–12488.
- [4] Z. Yi, J. Ye, N. Kikugawa, T. Kako, S. Ouyang, H. Stuart-Williams, H. Yang, J. Cao, W. Luo, Z. Li, *Nat. Mater.* 9 (2010) 559–564.
- [5] C. Xu, Y. Liu, B. Huang, H. Li, X. Qin, X. Zhang, Y. Dai, *App. Surf. Sci.* 257 (2011) 8732–8736.
- [6] H. Dong, G. Chen, J. Sun, C. Li, Y. Yu, D. Chen, *Appl. Catal. B Environ.* 134–135 (2013) 46–54.
- [7] S. Ouyang, J. Ye, *J. Am. Chem. Soc.* 133 (2011) 7757–7763.
- [8] G. Dai, J. Yu, G. Liu, *J. Phys. Chem. C* 116 (2012) 15519–15524.
- [9] C. Yu, G. Li, S. Kumar, K. Yang, R. Jin, *Adv. Mater.* 26 (2014) 892–898.
- [10] A. Zhang, L. Zhang, H. Lu, G. Chen, Z. Liu, J. Xiang, L. Sun, *J. Hazard. Mater.* 314 (2016) 78–87.
- [11] L. Shi, L. Liang, F. Wang, M. Liu, J. Sun, *J. Mater. Sci.* 50 (2015) 1718–1727.
- [12] S.B. Rawal, S.D. Sung, W.I. Lee, *Catal. Commun.* 17 (2012) 131–135.
- [13] C. Yu, L. Wei, J. Chen, Y. Xie, W. Zhou, Q. Fan, *Ind. Eng. Chem. Res.* 53 (2014) 5759–5766.
- [14] N. Mohaghegh, B. Eshaghi, E. Rahimi, M.R. Gholami, *J. Mol. Catal. A: Chem.* 406 (2015) 152–158.
- [15] L. Xu, W. Huang, L. Wang, G. Huang, P. Peng, *J. Phys. Chem. C* 118 (2014) 12972–12979.
- [16] J. Xu, Z. Gao, K. Han, Y. Liu, Y. Song, *ACS Appl. Mater. Interfaces* 6 (2014) 15122–15131.
- [17] X. Tao, Q. Hong, T. Xu, F. Liao, *J. Mater. Sci. Mater. Electron.* 25 (2014) 3480–3485.
- [18] Y. Song, J. Zhu, H. Xu, C. Wang, Y. Xu, H. Ji, K. Wang, Q. Zhang, H. Li, *J. Alloys Compd.* 592 (2014) 258–265.
- [19] C. Yu, L. Wei, W. Zhou, J. Chen, Q. Fan, H. Liu, *Appl. Surf. Sci.* 319 (2014) 312–318.
- [20] X. Guan, L. Guo, *ACS Catal.* 4 (2014) 3020–3026.
- [21] Q. Zhu, W. Wang, L. Lin, G. Gao, H. Guo, H. Du, A. Xu, *J. Phys. Chem. C* 117 (2013) 5894–5900.
- [22] P. Dong, Y. Wang, B. Cao, S. Xin, L. Guo, J. Zhang, F. Li, *Appl. Catal. B Environ.* 132–133 (2013) 45–53.
- [23] Y. Hou, X. Li, Q. Zhao, G. Chen, C.L. Raston, *Environ. Sci. Technol.* 46 (2012) 4042–4050.
- [24] J. Xie, Y. Yang, H. He, D. Cheng, M. Mao, Q. Jiang, L. Song, J. Xiong, *Appl. Surf. Sci.* 355 (2015) 921–929.
- [25] Y. Wang, P. Ren, C. Feng, X. Zheng, Z. Wang, D. Li, *Mater. Lett.* 115 (2014) 85–88.
- [26] C. Feng, G. Li, P. Ren, Y. Wang, X. Huang, D. Li, *Appl. Catal. B Environ.* 158–159 (2014) 224–232.
- [27] C. Feng, Y. Pang, Y. Wang, M. Sun, C. Zhang, L. Zhang, Y. Zhou, D. Li, *Appl. Surf. Sci.* 376 (2016) 188–198.
- [28] C. Feng, Y. Wang, J. Zhang, L. Yu, D. Li, J. Yang, Z. Zhang, *Appl. Catal. B Environ.* 113–114 (2012) 61–71.
- [29] A.E. Regazzoni, P. Mandelbaum, M. Matsuyoshi, S. Schiller, S.A. Bilmes, M.A. Blesa, *Langmuir* 14 (1998) 868–874.
- [30] Y. Wang, C. Feng, M. Zhang, J. Yang, Z. Zhang, *Appl. Catal. B Environ.* 100 (2010) 84–90.
- [31] H. Yu, W. Chen, X. Wang, Y. Xu, J. Yu, *Appl. Catal. B Environ.* 187 (2016) 163–170.
- [32] C. Yu, K. Yang, Q. Shu, J.C. Yu, F. Cao, X. Li, X. Zhou, *Sci. Chin. Chem.* 55 (2012) 1802–1810.
- [33] G. Dai, J. Yu, G. Liu, *J. Phys. Chem. C* 115 (2011) 7339–7346.
- [34] R.T. Sanderson, *Chemical Periodicity*, Reinhold, New York, 1960.
- [35] Y. Dian, C. Zhida, W. Fan, L. Shuzhou, *Acta Phys. Chim. Sin.* 17 (2001) 15–22.
- [36] F. Delogu, *Mater. Chem. Phys.* 137 (2012) 297–302.
- [37] G. Ligios, A.M. Bertetto, F.J. Delogu, *J. Alloys Compd.* 554 (2013) 426–431.
- [38] F. Delogu, *Langmuir* 28 (2012) 10898–10904.
- [39] J.E. Lee, S. Bera, Y.S. Choi, W.I. Lee, *Appl. Catal. B Environ.* 214 (2017) 15–22.
- [40] D. Chen, Q. Chen, L. Ge, L. Yin, B. Fan, H. Wang, H. Lu, H. Xu, R. Zhang, G. Shao, *Appl. Surf. Sci.* 284 (2013) 921–929.
- [41] K. Awazu, M. Fujimaki, C. Rockstuhl, J. Tominaga, H. Murakami, Y. Ohki, N. Yoshida, T. Watanabe, *J. Am. Chem. Soc.* 130 (2008) 1676–1680.
- [42] S. Zargari, R. Rahimi, A. Ghaffarinejad, A. Morsali, *J. Colloid Interface Sci.* 466 (2016) 310–321.
- [43] M. Sookhakian, Y.M. Amin, R. Zakaria, W.J. Basirun, M.R. Mahmoudian, B. Nasiri-Tabrizi, S. Baradaran, M. Azarang, *J. Alloys Compd.* 632 (2015) 201–207.
- [44] K. Awazu, M. Fujimaki, C. Rockstuhl, J. Tominaga, H. Murakami, Y. Ohki, N. Yoshida, T. Watanabe, *J. Am. Chem. Soc.* 130 (2008) 1676–1680.
- [45] W. Fa, P. Wang, B. Yue, F. Yang, D. Li, Z. Zhang, *Chin. J. Catal.* 36 (2015) 2186–2193.
- [46] X. Wang, M. Utsumi, Y. Yang, D. Li, Y. Zhao, Z. Zhang, C. Feng, N. Sugiura, J.J. Cheng, *Appl. Surf. Sci.* 325 (2015) 1–12.
- [47] L. Di, Z. Xu, X. Zhang, *Catal. Today* 211 (2013) 143–146.
- [48] D. Wang, Z.-H. Zhou, H. Yang, K.-B. Shen, Y. Huang, S. Shen, *J. Mater. Chem.* 22 (2012) 16306.
- [49] Z. Liu, W. Hou, P. Pavaskar, M. Aykol, S.B. Cronin, *Nano Lett.* 11 (2011) 1111–1116.
- [50] L. Kuai, B. Geng, X. Chen, Y. Zhao, Y. Luo, *Langmuir* 26 (2010) 18723–18727.
- [51] L. Sun, J. Li, C. Wang, S. Li, Y. Lai, H. Chen, C. Lin, *J. Hazard. Mater.* 171 (2009) 1045–1050.
- [52] E. Kowalska, R. Abe, B. Ohtani, *Chem. Commun.* (2009) 241–243.
- [53] Y. Zhao, B. Yang, J. Xu, Z. Fu, M. Wu, F. Li, *Thin Solid Films* 520 (2012) 3515–3522.
- [54] C. Hu, Y. Lan, J. Qu, X. Hu, A. Wang, *J. Phys. Chem. B* 110 (2006) 4066–4072.
- [55] X. Zhou, C. Hu, X. Hu, T. Peng, J. Qu, *J. Phys. Chem. C* 114 (2010) 2746–2750.
- [56] J. Wen, X. Li, W. Liu, Y. Fang, J. Xie, Y. Xu, *Chin. J. Catal.* 36 (2015) 2049–2070.
- [57] D. Chen, Q. Chen, L. Ge, L. Yin, B. Fan, H. Wang, H. Lu, H. Xu, R. Zhang, G. Shao, *Appl. Surf. Sci.* 284 (2013) 921–929.